Modelling the dispersion and transport of reactive pollutants in a deep urban street canyon

Zhong, Jian; Cai, Xiaoming; Bloss, William

DOI:
10.1016/j.envpol.2015.02.009

Modelling the dispersion and transport of reactive pollutants in a deep urban street canyon: Using large-eddy simulation

Jian Zhong, Xiao-Ming Cai* and William James Bloss

School of Geography, Earth & Environmental Sciences, University of Birmingham, Edgbaston, Birmingham, B15 2TT, UK

**Corresponding author*. Tel.: (0121) 4145533; Fax: (0121) 4145528.

Email address: x.cai@bham.ac.uk (X.-M. Cai).

Abstract:

This study investigates the dispersion and transport of reactive pollutants in a deep urban street canyon with an aspect ratio of 2 under neutral meteorological conditions using large-eddy simulation. The spatial variation of pollutants is significant due to the existence of two unsteady vortices. The deviation of species abundance from chemical equilibrium for the upper vortex is greater than that for the lower vortex. The interplay of dynamics and chemistry is investigated using two metrics: the photostationary state defect, and the inferred ozone production rate. The latter is found to be negative at all locations within the canyon, pointing to a systematic negative offset to ozone production rates inferred by analogous approaches in environments with incomplete emission mixing. This study demonstrates an approach to quantify parameters for a simplified two-box model, which could support traffic management and urban planning strategy or personal exposure assessment.

Capsule:

Reactive pollutants in a deep street canyon exhibit significant spatial variation driven by two unsteady vortices. A method of quantifying parameters of a two-box model is developed.

Keywords:

Urban street canyon, Large-eddy simulation, Pollutant removal, Turbulence, Two-box model.

1 Introduction

The term “street canyon” describes a restricted space (poor air ventilation) with surrounding buildings along both sides of the urban street. Vehicle emissions are dominant among various anthropogenic pollutant sources in urbanized areas (Liu et al., 2005). A combination of vehicle emissions and reduced dispersion caused by surrounding buildings could result in poor air quality at the pedestrian level, thereby leading to associated public health effects for those exposed to such environments (Solazzo et al., 2011). Understanding the dispersion and transport of reactive pollutants in urban street canyons is important to effectively quantify – and develop policies to mitigate – such impacts.

Various approaches have been undertaken over recent years to tackle the issue of air pollution inside street canyons. The most fundamental approach is direct field measurement, which can provide the first-hand and useful information. Examples of such approach include the studies by Xie et al. (2003), Kumar et al. (2008) and Prajapati et al. (2009). However, there are several disadvantages of field measurements, e.g. challenges to data interpretation, uncontrollable meteorological conditions, low spatial coverage, and high expense. An alternative approach is physical modelling, such as wind tunnels, e.g. Sagrado et al. (2002), Kovar-Panskus et al. (2002), Park et al. (2004) and Michioka et al. (2011), and water channels, e.g. Caton et al. (2003), Jiang et al. (2007) and Li et al. (2008a). Physical modelling offers the advantages of fully controlling testing parameters and sampling points so as to provide useful data for the evaluation of numerical models. However, there is a challenge for such models to replicate fully the large-scale atmospheric turbulence of the real world due to the scale limitation. Another useful alternative approach is numerical simulation (e.g. computational fluid dynamics, CFD). With rapid development of advanced computer technology, CFD has become a useful tool to explore experimental flow and pollutant dispersion problems (Chang, 2006), providing a complete view of distribution of flow and pollutant fields at high-resolution in both time and space. The most comprehensive applications of CFD have been based on Reynolds-averaged Navier–Stokes (RANS) equations and large-eddy

simulation (LES). RANS can only predict mean information about the flow and pollutant fields, while LES also provides the turbulent information about unsteadiness and intermittency (Cai et al., 2008).

The flow patterns in a street canyon under neutral meteorological conditions can be classified into three main regimes (Oke, 1987): isolated roughness, wake interference and skimming flow, depending on the aspect ratio (AR, the ratio of building height H to street width W). Skimming flow, which has been the subject of several studies and will be further investigated here, normally occurs in the regular street canyons ($0.7<AR<1.5$) and deep street canyons ($AR > 1.5$) (Murena et al., 2009). A single primary vortex is formed within the regular street canyon (e.g. AR=1), which has been extensively studied. Most studies only considered passive pollutants (i.e. non-reactive scalars). However, vehicle emissions are chemically reactive, evolving on the timescale of typical canyon circulation and residence times. Such chemical processes are expected to play a role in determining abundance, alongside dispersion and transport, of reactive pollutants. Baker et al. (2004) introduced simple NO_x-O_3 chemistry into a LES model and examined reactive pollutant dispersion and transport inside a regular street canyon (AR=1). The concept of the photostationary state (PSS) defect was introduced and served as a sensitive indicator of reactive mixing. Baik et al. (2007) carried out a RANS model of a regular street canyon (AR=1) using the same chemistry as the study by Baker et al. (2004). Both these studies showed that the chemistry is close to equilibrium within the primary canyon vortex, but far from equilibrium at the canyon roof level where air exchange between the canyon and the overlying background takes place. Kikumoto and Ooka (2012) investigated the transport and dispersion of atmospheric pollutants within a regular street canyon (AR=1) by using LES coupled with a bimolecular chemical reaction ($O_3 + NO \rightarrow$ product). They found that NO_x and O_3 have contrasted mechanism of transport and the correlation between the reactants' concentration fluctuations strongly influences the reaction rates at the canyon roof level. Kwak and Baik (2012) and Kwak et al. (2013) employed a RANS model coupled with the carbon bond mechanism IV (CBM-IV) considering the chemistry of O_3, NO_x and volatile organic

compounds (VOCs) in idealized street canyons (AR=1,2). They found that both O_3 and OH oxidation processes are of vital importance in the canyon-scale chemistry and that there are two counter-rotating vortices in the street canyon with AR=2. According to Li et al. (2009), there are multiple vortices within a deep street canyon, which may create very poor ventilation conditions for pollutants. Thus the dispersion of pollutants in a deep street canyon could be substantially different from the AR=1 case, very complex in terms of both dynamical and chemical processing, and deserves a thorough examination.

This study investigates the dispersion and transport of reactive pollutants in a deep urban street canyon (AR=2). The LES methodology coupled with a simple chemical mechanism is employed as described in Section 2. In Section 3, the results of the LES dynamical model are evaluated against a water-channel experiment, and the characteristics of reactive pollutant dispersion from the LES coupled with the simple NO_x-O_3 chemistry are presented. A two-box model framework is developed. Finally, the conclusions are presented in Section 4.

2 Methodology

2.1 Numerical model

2.1.1 Flow equations

The LES model employed here is OpenFoam v2.1.1 (OpenFOAM, 2012), in which incompressible flow and neutral condition are assumed. The filtered momentum equations and continuity equations are

$$\frac{\partial \overline{u}_i}{\partial t} + \frac{\partial}{\partial x_j}\overline{u}_i\overline{u}_j = -\Delta P\delta_{i1} - \frac{\partial \overline{p}}{\partial x_i} - \frac{\partial \tau_{ij}}{\partial x_j} + \upsilon\frac{\partial^2 \overline{u}_i}{\partial x_j \partial x_j} \quad (1)$$

$$\frac{\partial \overline{u}_i}{\partial x_i} = 0 \quad (2)$$

where the overbar ($\bar{\bullet}$) represents the filtered quantity, $\bar{u}_i$ (i=1,2,3) are the filtered velocities, ΔP is the large-scale kinematic pressure difference, δ_{ij} is the Kronecker delta, $\bar{p}$ is the filtered kinematic pressure, υ is the kinematic molecular viscosity and τ_{ij} represents the sub-grid scale (SGS) stresses, which are parameterised as follows:

$$\tau_{ij} = -2\upsilon_{SGS} S_{ij} \tag{3}$$

$$S_{ij} = \frac{1}{2}\left(\frac{\partial \bar{u}_i}{\partial x_j} + \frac{\partial \bar{u}_j}{\partial x_i}\right) \tag{4}$$

$$\upsilon_{SGS} = C_k k_{SGS}^{1/2} \Delta \tag{5}$$

$$\Delta = (\Delta_1 \Delta_2 \Delta_3)^{1/3} \tag{6}$$

$$\frac{\partial k_{SGS}}{\partial t} + \frac{\partial}{\partial x_i}(k_{SGS}\bar{u}_i) = 2\upsilon_{SGS} S_{ij} S_{ij} + (\upsilon + \upsilon_{SGS})\frac{\partial^2 k_{SGS}}{\partial x_i \partial x_i} - C_\varepsilon \frac{k_{SGS}^{3/2}}{\Delta} \tag{7}$$

where k_{SGS} is the SGS turbulent kinetic energy, Δ_i (i=1,2,3) are the local grid spacings and the modelling constants $C_k = 0.094$, $C_\varepsilon = 1.048$.

The study simulates the high Reynolds number (~10^6) turbulent flow (see Section 2.2) in a deep street canyon with rough surfaces and the logarithmic law of the rough-wall (Schlichting and Gersten, 2000) is applied for the near-wall treatment:

$$\bar{u}_{\parallel} = \frac{u_\tau}{\kappa} \ln \frac{z_\perp}{z_0} \tag{8}$$

where $\bar{u}_{\parallel}$ is the resolved scale velocity component parallel to the wall, u_τ is the wall friction velocity, κ (=0.42) is the von Kármán constant, $z_\perp$ is the distance normal to the wall and z_0 (=0.015 m representing a characteristic physical length of 0.15 m, e.g. window frames) is the aerodynamic surface roughness length. u_τ is calculated by Equation (8) and used to derive υ_{SGS} near the wall using

$$\upsilon_{SGS} = \frac{u_\tau^2}{|\nabla \overline{u}_\parallel \cdot \hat{n}|} - \upsilon \quad (9)$$

where $\hat{n}$ is the unit vector normal to the wall.

2.1.2 Equations for reactive pollutants

The reactive pollutants concerned here are nitric oxide (NO), nitrogen dioxide (NO_2) and ozone (O_3). The associated chemical reactions are (Carpenter et al., 1998):

$$NO_2 + h\nu \rightarrow NO + O \quad (10)$$

$$O + O_2 + M \rightarrow O_3 + M \quad (11)$$

$$O_3 + NO \rightarrow NO_2 + O_2 \quad (12)$$

where M denotes a third body molecule (usually O_2 or N_2) which absorbs excess energy so that O and O_2 may recombine to form an O_3 molecule. The filtered equations for the concentrations of reactive pollutants are:

$$\frac{\partial[\overline{NO}]}{\partial t} + \frac{\partial}{\partial x_i}(\overline{u}_i[\overline{NO}]) = \frac{\partial}{\partial x_i}([\frac{\upsilon + \upsilon_{SGS}}{Sc}] \cdot \frac{\partial[\overline{NO}]}{\partial x_i}) + J_{NO_2}[\overline{NO_2}] - k_1[\overline{O_3}][\overline{NO}] + S_{NO} \quad (13)$$

$$\frac{\partial[\overline{NO_2}]}{\partial t} + \frac{\partial}{\partial x_i}(\overline{u}_i[\overline{NO_2}]) = \frac{\partial}{\partial x_i}([\frac{\upsilon + \upsilon_{SGS}}{Sc}] \cdot \frac{\partial[\overline{NO_2}]}{\partial x_i}) - J_{NO_2}[\overline{NO_2}] + k_1[\overline{O_3}][\overline{NO}] + S_{NO_2} \quad (14)$$

$$\frac{\partial[\overline{O_3}]}{\partial t} + \frac{\partial}{\partial x_i}(\overline{u}_i[\overline{O_3}]) = \frac{\partial}{\partial x_i}([\frac{\upsilon + \upsilon_{SGS}}{Sc}] \cdot \frac{\partial[\overline{O_3}]}{\partial x_i}) + k_2[\overline{O}][\overline{O_2}][\overline{M}] - k_1[\overline{O_3}][\overline{NO}] \quad (15)$$

where J_{NO_2} is the photolysis rate for NO_2 in Reaction (10); k_1 and k_2 are the rate constants for Reactions (11) and (12), respectively; S_{NO} and S_{NO_2} are the emission rates for NO and NO_2, respectively; *Sc* (=0.72) is the Schmidt number. Based on the pseudo-steady-state approximation for the highly reactive oxygen atom (O) (Seinfeld and Pandis, 1998), the formation rate of O by

136 Reaction (10) is the same as the depletion rate of O by Reaction (11). Thus, the following equation
137 is derived:

138 $$k_2[\overline{O}][\overline{O_2}][\overline{M}] = J_{NO_2}[\overline{NO_2}]. \quad (16)$$

139 Therefore, substituting Equation (16) into Equation (15) yields:

140 $$\frac{\partial[\overline{O_3}]}{\partial t} + \frac{\partial}{\partial x_i}(\overline{u_i}[\overline{O_3}]) = \frac{\partial}{\partial x_i}([\frac{\upsilon + \upsilon_{SGS}}{Sc}]\cdot\frac{\partial[\overline{O_3}]}{\partial x_i}) + J_{NO_2}[\overline{NO_2}] - k_1[\overline{O_3}][\overline{NO}] \quad (17)$$

141 For further analysis, the photostationary state (PSS) defect d_{ps} (Baker et al., 2004) is defined:

142 $$d_{ps}(\%) = (\frac{k_1[\overline{O_3}][\overline{NO}]}{J_{NO_2}[\overline{NO_2}]} - 1)\times 100, \quad (18)$$

143 where the values of J_{NO_2} and k_1 are 0.0092 s^{-1} and 0.0004 ppb^{-1} s^{-1}, respectively (Bright et al., 2013).
144 d_{ps} is a widely-used measure of the deviation from chemical equilibrium. The larger is the
145 magnitude of d_{ps}, the higher is the deviation from the chemical equilibrium. $d_{ps} = 0$ means that the
146 chemistry is at the equilibrium state.

147 We may also define PO_3 as the ozone production rate associated with the VOCs chemistry under the
148 perfect mixing condition as follows. Atmospheric chemical reactions of hydro- and organic-peroxy
149 radicals (HO_2 *and* RO_2) with NO generate NO_2 through:

150 $$NO + HO_2 \rightarrow NO_2 + OH \quad (19)$$

151 $$NO + RO_2 \rightarrow NO_2 + RO \quad (20)$$

152 Considering a chemical equilibrium system with perfect mixing comprising Reactions (10)-(12),
153 (19) and (20), we obtain

154 $$J_{NO_2}[NO_2] - k_1[O_3][NO] = k_3[NO][HO_2] + \sum_i k_{4,i}[NO][RO_2]_i \quad (21)$$

where k_3 and $k_{4,i}$ are the rate constants for Reactions (19) and (20), respectively; *i* is the i^{th} organic-peroxy radical. The terms $k_3[NO][HO_2] + \sum_i k_{4,i}[NO][RO_2]_i$ represent the rate of conversion of NO to NO_2 (through the VOCs chemistry) which is subsequently photolysed leading to O_3 production. Thus we define $PO_3 = k_3[NO][HO_2] + \sum_i k_{4,i}[NO][RO_2]_i$. Due to the difficulties of evaluating HO_2 and RO_2 from measurement, we may use (21) to infer PO_3 from the NO_x and O_3 measurements:

$$PO_3 = J_{NO_2}[\overline{NO_2}] - k_1[\overline{O_3}][\overline{NO}], \quad (22)$$

This is referred to as the NO_x-O_3-steady-state-defect approach. In this approach, we assume that deviations from PSS arising from imperfect mixing are negligible (Volz-Thomas et al., 2003). We evaluate the accuracy of this assumption within the canyon environment in Section 3.2.1.

2.2 Model configuration and initialisation

Fig.1 illustrates schematically the computational domain of an idealised deep street canyon (AR=2, i.e. $H = 36\ m$ and $W = 18\ m$). The building width *B* is 18 m. The domain width sizes $(L_x \times L_y \times L_z)$ are $36\ m \times 40\ m \times 112\ m$. The grid resolutions $(\Delta x \times \Delta y \times \Delta z)$ are $0.3\ m \times 1\ m \times 0.3\ m$, with Δz gradually increasing from 0.3 m at the canyon roof level to a maximum value of 5.54 m at the top. The number of grid cells in the *x*- , *y*- and *z*-directions is $60 \times 40 \times 120$ within the canyon and $120 \times 40 \times 40$ above the canyon, respectively.

A constant pressure gradient (ΔP) across the free surface layer (above the canyon) is imposed in the *x*-direction to drive the atmospheric flow (perpendicular to the street axis), representing the worst-case scenario for the dispersion of reactive pollutants within a street canyon (Li et al., 2008b). The prevailing wind speed U_f is about 2.2 m s^{-1} and the Reynolds number Re $(= U_f H / \nu)$ is the order of 10^6. For velocity components, the symmetry boundary condition is employed at the domain top. Cyclic boundary conditions are specified in both the *x*- and *y*- directions. Therefore, the model

178 configuration represents an infinite number of idealised street canyons along the *x*-direction and
179 each canyon is infinitely long in the *y*-direction, which is a good approximation of real street
180 canyons relevant to traffic management or urban planning.

181 Emissions sources are assumed to be two continuous line sources representing two lanes of traffic
182 located at 2.5 m from both sides of the canyon centre at $z = 1\ m$ with a Gaussian distribution (i.e.
183 $\delta_x = 3\ m$ and $\delta_z = 1\ m$) so that the near-vehicle dispersion is approximated. Drawing upon the UK
184 Road Vehicle Emission Factors (Boulter et al., 2009b), the emission rate of NO_x is determined as
185 620 g km^{-1} h^{-1}, which represents an urban continuous road traffic of 1500 vehicles h^{-1} with an
186 average speed of 30 mph for a fleet composition representing the year of 2010 (Zhong et al., 2014).
187 The total emission for NO_x applied here is equivalent to 1000 ppb s^{-1} released into a typical LES
188 model grid ($0.3\ m \times 1\ m \times 0.3\ m$) but this total emitted NO_x is re-distributed based on the Gaussian
189 distribution mentioned above. The ratio of NO to NO_2 emission rate is 9:1 by volume. The
190 background concentrations of NO, NO_2 and O_3 used are 3.07, 6.02 and 43.62 ppb (Bright et al.,
191 2013), respectively, which are uniformly distributed among the whole domain initially and also
192 employed as the inlet boundary conditions, i.e. signifying no emissions from upwind canyons. For
193 the outlet, the advective boundary condition (i.e. $\frac{\partial \overline{c}_i}{\partial t} + \overline{u}\frac{\partial \overline{c}_i}{\partial x} = 0$) is applied, representing no
194 reflection of pollutants back into the computational domain. For the solid boundaries, zero-gradient
195 boundaries are applied without considering the effect of pollutant deposition. The symmetry
196 boundary is set on the top boundary and a cyclic boundary condition is adopted in the *y*- direction
197 for the pollutants.

198 Initially, the LES model is run with dynamics only for 5 hours in order to generate a statistically
199 steady turbulent flow turbulent flow. We take the dynamical-equilibrium flow field as the initial
200 condition (i.e. $t = 0$ min) for the model in this study and further run the LES model without
201 chemistry for the first 30 min before considering chemistry. At $t = 30$ min, the chemistry scheme

and emissions modules are turned on for the next 210 min ($t = 30\ to\ 240$ min) with a time step of 0.03 s in order to reach chemical quasi-equilibrium. For the analysis, the simulation 3-D outputs over the last 60 min period ($t = 180\ to\ 240$ min) at a time interval of 3 s are stored and post-processed to derive the resolved-scale turbulent statistics based on the averages over the period and along the *y*-direction. This temporal average over $t \in [t_1, t_2]$ and spatial average over $y \in [0, L_y]$ of any quantity $\bar{\phi}(=\langle\bar{\phi}\rangle + \phi')$ gives $\langle\bar{\phi}\rangle$, which is a 2D function of (*x*,*z*):

$$\langle\bar{\phi}\rangle(x,z) = \frac{1}{L_y(t_2 - t_1)} \int_{t_1}^{t_2} \int_0^{L_y} \bar{\phi}(x,y,z,t)\,dy\,dt \tag{23}$$

and the fluctuation component ϕ' is described as follows:

$$\phi'(x,z) = \frac{1}{L_y(t_2 - t_1)} \int_{t_1}^{t_2} \int_0^{L_y} [\bar{\phi}(x,y,z,t) - \langle\bar{\phi}\rangle(x,z)]\,dy\,dt \tag{24}$$

3 Results and discussion

3.1 Flow field

A water-channel experiment (Li et al., 2008a) is employed to evaluate the performance of the current LES simulation with respect to the flow field. This water-channel experiment was conducted in a laboratory flume, which was 10 m in length, 0.3 m in width and 0.5 m in height. Several identical building blocks ($0.1\ m \times 0.3\ m \times 0.1\ m$ in the *x*-, *y*- and z- directions) were placed perpendicular to the flow with the street width of 0.05 m (i.e. AR=2). The laser Doppler anemometer technique was applied for the data acquisition of the velocities and turbulent statistics.

Fig. 2 shows the comparison of vertical profiles of the normalized averaged streamwise and vertical velocities and their fluctuation intensities at the upstream, centre and downstream locations for the deep street canon (AR=2) between the current LES simulation and the water-channel experiment.

All of the quantities in Fig. 2 are normalized by u_{norm} (the averaged value of $\langle \bar{u} \rangle$ at the height $1.0 \le z/H \le 1.1$). Fig 2a presents the mean streamwise velocity and there is clear evidence of a shear layer across the canyon roof level, at which strong wind shear strength is observed. Fig. 2b shows the vertical mean velocities and there is clear evidence of the complicated flow pattern: the clockwise vortex in the upper part of the canyon and the weak anti-clockwise vortex in the lower part of the canyon. The upper recirculation is created by the strong wind shear at the roof level and the lower recirculation is generated by a relatively weaker wind shear induced by the upper recirculation. Figs. 2c and 2d illustrate the intensity of resolved-scale fluctuations of the two velocity components, which display local maxima at the canyon roof level. These maxima may be caused by the instability of the wind shear-layer at the canyon roof level. As shown in Fig. 2, there are some small discrepancies between the current LES simulation and the water-channel experiment. The current LES simulation generally slightly underestimates all the quantities. There are several possible reasons for this. Firstly, due to the computational cost, a limited computational domain is employed in the current LES simulation, only representing eddies with sizes smaller than half of the domain width. However, eddies in the experiment are created by the vortex generators and there may be larger eddies which are not modelled in the LES simulation. Secondly, the grid mesh might not be fine enough across the shear-layer, and so some small eddies within the shear-layer and the momentum exchange caused by these small eddies might not be resolved. Finally, these discrepancies may be attributed to different averaging approaches. In the LES simulation, the temporal and spatial averaging approach is adopted to derive the flow quantities. In the experiment, these quantities were only measured on a middle vertical plane in the *y*- direction (Li et al., 2008a).

Fig. 3 illustrates the vortex structure in the current LES simulation compared with a wind tunnel experiment carried out by Kovar-Panskus et al. (2002). Both the model and experiment shows that there are two counter-rotating vortices formed within the deep street canyon (AR=2). This is a major difference from the single-vortex flow for a street canyon with AR=1 (e.g. Bright et al., 2013). The two-vortex mean flow was also found by other studies for AR=2 using RANS, e.g.

Kwak et al. (2013), but their RANS model generated a larger lower vortex than the one found in the water tank experiment and in the LES result here. It is also noted that the upper vortex is centred lower within the canyon compared with the experiment. Also, the centre of the lower vortex is shifted downstream closer to the windward wall compared with that of the upper vortex both in the model and experiment.

Overall, the current LES simulation agrees well with the experiments in terms of the velocities, turbulent intensities and vortex structure, which provides confidence that the simulated dynamics within the canyon is reasonable. However, there are currently no suitable water-channel or wind-tunnel experiments to evaluate the dispersion of reactive species, especially in deep street canyons.

3.2 Pollutant dispersion and transport

3.2.1 Spatial variation of reactive pollutants

Figs. 4a-f depict contour plots of the spatially and temporally averaged mixing ratios of (a) $\langle \overline{NO} \rangle$, (b) $\langle \overline{NO_2} \rangle$, (c) $\langle \overline{O_3} \rangle$, (d) $\langle \overline{NO_x} \rangle$, (e) $\langle \overline{O_x} \rangle$, and (f) $\langle \overline{NO} \rangle / \langle \overline{NO_2} \rangle$. The plots show the influence of two primary vortices, which span the deep street canyon: the upper clockwise vortex, and the lower anti-clockwise vortex. This influence was also found by Kwak et al. (2013) for the street canyon with AR=2. In general, the spatial patterns of the quantities for the upper vortex resemble those for the single vortex in a street canyon with AR=1, e.g. Baker et al. (2004), Baik et al. (2007), Bright et al., 2013, Garmory et al. (2009), Tong and Leung (2012), and Kwak and Baik (2012). There also exist two shear layers. The first one is at the canyon roof level with increasing turbulence from the leeward (upwind) building to the windward (downwind), which traps NO_x emissions near the leeward building, allows more exchange near the windward building and entrains O_3 into the canyon toward the windward building. The other one is at the level of around z/W=0.5, which allows the NO_x emissions generated at the ground level inside the lower vortex to intrude into the upper vortex and the ambient O_3 inside the upper vortex to be entrained into the lower vortex. NO_x

and O_3 are allowed to mix and react with each other inside the two vortices in the presence of the two shear layers where exchanges take place. It is also noted that there is an accumulation of traffic emissions with a maximum value of about 1100 ppb for NO_x and a low level of O_3 with a minimum value of about 4 ppb in the lower vortex. This is attributed to a high level of NO_x emitted into the very weak lower vortex to react with the limited O_3 entrained along the windward wall from above. This is very different from what Kwak et al. (2013) showed in their Fig. 2(d) which gives a local maximum of about 30 ppb near the centre of the lower vortex. One explanation is that their emission rate of NO_x is much lower than ours (20 vs. 90 ppb s^{-1} released into 1 m^3). Considering the NO_x-O_3 photochemistry, $NO_x = (NO + NO_2)$ and the total oxidant $O_x = (O_3 + NO_2)$ are effectively passive, exhibiting a similar spatial distribution to each other. The ratio of NO/NO_2 also shows a similar pattern across the two vortices ranging from about 6 at the right corner to about 3 at the canyon roof level, which indicates the conversion of NO to NO_2 by the within-canyon chemistry. Figs. 4g-h show contour plots of the spatially and temporally averaged d_{ps} and PO_3. The magnitudes of d_{ps} and PO_3 are smaller in the lower vortex than that in the upper vortex indicating that there is greater mixing for the chemistry system to reach the chemical equilibrium in the lower vortex compared to that in the upper vortex. This can be explained by the weaker vortex in the lower part of the canyon, where time scale is adequate to approach chemical equilibrium. A local maxima in d_{ps} (about 150%) and PO_3 (about -0.68 ppb s^{-1}) are observed across the canyon roof level in the presence of the strong turbulence. It is also observed that there are significantly larger values of d_{ps} and PO_3 along the upper part of the windward building, indicating larger deviation from photochemical equilibrium in the region where two air parcels with very different chemical compositions interact.

Fig. 5 illustrates vertical profiles of (a) $\langle \overline{NO} \rangle$, (b) $\langle \overline{NO_2} \rangle$, (c) $\langle \overline{O_3} \rangle$, (d) $\langle \overline{NO_x} \rangle$, (e) $\langle \overline{O_x} \rangle$, (f) $\langle \overline{NO} \rangle / \langle \overline{NO_2} \rangle$, (g) d_{ps} and (h) PO_3 along the leeward and windward walls. These quantities are

296 averaged within the nearest three cells adjacent to the walls. The concentrations of NO, NO_2, NO_x,
297 O_x and NO/NO_2 on the leeward wall are higher (around 1.5 to 2 times) than those on the windward
298 wall within the upper part of the canyon, but lower (around 50% to 70%) within the lower part. This
299 indicates that traffic emissions are mainly trapped within the anti-clockwise lower vortex. For O_3,
300 the situation is reversed with much lower values on the leeward wall (around 6 ppb) compared to
301 those on the windward wall (ranging from about 6 ppb to 20 ppb) within the upper part of the
302 canyon, but with slightly higher values (about 2 ppb difference) within the lower part. This is
303 attributed to ambient O_3 being brought into the upper part of canyon along the windward wall. It is
304 also noted that the concentration reduces with height by a factor of about 0.8 on the leeward wall
305 and by a factor of about 0.1 on the leeward wall for NO, NO_2, NO_x, O_x and NO/NO_2, but increases
306 by a factor of about 1.3 on the leeward wall and by a factor of about 5.5 on the leeward wall for O_3.
307 For the leeward wall, there is a sharp transition at the canyon roof level where each species rapidly
308 approaches its background level, and a small gradient in concentration within the canyon. For the
309 windward wall, there are two gradual transitions at the roof level and at the middle level of the
310 canyon, respectively. These results for the upper part of the canyon match those of the field
311 measurements by Xie et al. (2003), in which there was only one primary vortex inside the street
312 canyon. The magnitudes of d_{ps} and PO_3 are very small (around 3% and 0.03 ppb s^{-1}, respectively)
313 along the leeward wall inside the canyon, but increase rapidly within the shear layer at the roof level
314 (around 80% and 0.40 ppb s^{-1}, respectively), where two air parcels with different compositions
315 interact. Along the windward wall, the magnitudes of d_{ps} and PO_3 increase with height with much
316 higher values in the upper part of the canyon, ranging from about 10% to 140% and from -0.08 ppb
317 s^{-1} to -0.53 ppb s^{-1} , respectively. This indicates that the deviation from chemical equilibrium is
318 much larger in the upper vortex than that in the lower vortex.

319 Fig. 6 illustrates vertical profiles of the spatially and temporally averaged total, turbulent and
320 advective fluxes, defined as $F_{total} = F_{turb} + F_{adv} = \langle w'\phi' \rangle (x,z) + \langle \overline{w} \rangle (x,z) \ \langle \overline{\phi} \rangle (x,z)$, for NO, NO_2, O_3,

NO_x, O_x and NO/NO_2 averaged across the canyon. It is interesting to note that the advective fluxes are dominant for both the upper and lower vortices while turbulent fluxes are dominant for the shear layers. It is observed that there is a positive (upward) total flux for NO and NO_2 from the canyon roof level into the background atmosphere aloft, and a negative (downward) total flux for O_3 indicating that O_3 is brought into the canyon from the overlying background atmosphere. A rapid increase in the total flux of NO and NO_2 is observed from the ground to the level at z/W=0.1. This is due to the elevation of traffic emissions from the ground level. The total flux generally decreases with height for NO, but increases for NO_2 indicating the conversion of NO to NO_2 within the canyon chemical processing before they escape to the wider background environment. This conversion is also indicated as the ratios of total fluxes of NO to NO_2 decrease with height from 9 near the emission source to about 4 at the canyon roof level. For the effective passive scalars NO_x and O_x, the total fluxes generally remain almost constant with height (around 5 ppb m s^{-1} for NO_x and 0.5 ppb m s^{-1} for O_x) except a rapid increase near the ground level.

In the model scheme used here, no peroxy radical reactions [Reactions (19) and (20)] are considered, i.e. *net* chemical ozone production cannot occur. Non-zero values for d_{ps}, therefore reflect the impact of imperfect mixing (heterogeneity) within the canyon, rather than ozone production chemistry. The values of PO_3 obtained here may therefore be regarded as measures of a systematic error in the NO_x-O_3-steady-state-defect approach to assess ozone production rates (via NO_x/O_3 measurements in the real atmosphere), i.e. indicating the magnitude of the imperfect-mixing-generated deviation from steady-state. The canyon averaged PO_3 = -0.074 ppb s^{-1} (i.e. -266 ppb h^{-1}) (see Fig. 4h) indicates a negative bias results at all locations, which is large compared with measured free boundary layer / free troposphere ozone production rates [typically a few ppb h^{-1}, up to 50 ppb h^{-1} in the most polluted regions, e.g. Mexico City (Wood et al., 2009)]. This reflects the fact that the PO_3 term effectively represents a small difference between two large quantities, such that the impact of mixing may be very substantial. In fact, this effect (imperfect mixing in the vicinity of NO_x emission sources) is general, and so a systematic negative contribution to NO_x-O_3-

steady-state derived ozone production rates will recur throughout the urban atmosphere, to an extent dependent upon the local heterogeneity.

3.2.2 Development of a two-box model

The preliminary results from the LES model show the formation of two primary counter-rotating vortices in the deep street canyon (AR=2), providing the potential to develop an alternative simplified two-box model. By using a plane at the level of z/W=0.5 (or z/H=0.25), the deep street canyon is divided into two boxes with the corresponding vortex inside each box (Figs. 3 and 7). It is assumed that each vortex has sufficient intensity for the chemical species to be well-mixed within the corresponding box (Murena et al., 2011). The mass transfer between two adjacent boxes is expressed by the introduction of an 'exchange velocity'. A one-box chemistry model has been previously adopted by Liu and Leung (2008) to study reactive pollutant dispersion in street canyons (AR=0.5, 1, 2), using the values of exchange velocity derived from LESs for different ARs. Because they treated the whole canyon as one well-mixed box for all ARs, the model is unable to reproduce the significant contrasts of pollutant concentration between the lower and upper canyon as shown in Fig. 4. In this study, a more complex box model (i.e. a two-box model) is adopted:

$$\frac{dc_{i,L}}{dt} = -\frac{w_{t,L}}{H_L}(c_{i,L} - c_{i,U}) + E_{i,L} + \Delta S_{i,L} \tag{25}$$

$$\frac{dc_{i,U}}{dt} = \frac{w_{t,L}}{H_U}(c_{i,L} - c_{i,U}) - \frac{w_{t,U}}{H_U}(c_{i,U} - c_{i,b}) + \Delta S_{i,U} \tag{26}$$

where $c_{i,L}$, $c_{i,U}$ and $c_{i,b}$ are concentrations of i^{th} species (i=NO, NO_2 and O_3) in the lower box, upper box and overlying background atmosphere, respectively; H_L and H_U are the heights of the lower and upper boxes, respectively; $w_{t,L}$ is the exchange velocity between the lower and upper boxes, and $w_{t,U}$ is the exchange velocity between the upper box and the overlying background

368 atmosphere; $\Delta S_{i,L}$ and $\Delta S_{i,U}$ are chemical sources of i^{th} species in the lower and upper boxes,
369 respectively; and $E_{i,L}$ is emission rates of i^{th} species.

370 Exchange velocities implemented into the two-box model are determined from the current LES
371 model by calculating the ventilation of a passive scalar, i.e. $w_{t,L} = \frac{F_L}{c_{ps,L} - c_{ps,U}}$ and
372 $w_{t,U} = \frac{F_U}{c_{ps,U} - c_{ps,b}}$, where F_L is the flux between the lower and upper boxes, F_U is the flux
373 between the upper box and the overlying background atmosphere and 'ps' denotes the passive
374 scalar. The resulting values applied into the two-box model are 0.018 m s^{-1} for $w_{t,L}$ and 0.014 m s^{-1}
375 for $w_{t,U}$. The two-box model is then compared with the LES model in terms of the time evolution
376 of the volume averaged mixing ratios of NO, NO_2, O_3, NO_x and O_x (see Fig. 8). There are apparent
377 fluctuations in the mixing ratios of chemical species inherent in the LES approach due to
378 dynamically-driven variability of large scale eddies and unsteady ventilation caused by the two
379 primary vortices in the canyon. The two-box model generally matches the LES approach with
380 respect to the mixing ratios for the lower box, but slightly underestimates for the upper box
381 compared with the LES results. This may attributed to the greater mixing for the lower vortex than
382 that for the upper vortex in the LES, indicated by the very small values for the PSS defects (Fig. 4g
383 and Fig. 5g).

384 ## 4 Conclusions

385 The dispersion and transport of reactive pollutants in a deep urban street canyon (AR=2) has been
386 examined using an LES model coupled with simple NO_x-O_3 photochemistry. It is observed that
387 there exist two vertically aligned vortices, agreeing reasonably well with a previous water channel
388 experiment. Reactive pollutants exhibit significant spatial variation caused by the two unsteady
389 vortices. Ground level sourced pollutants (NO_x) are found to be largely trapped within the lower

vortex with a maximum value of about 1100 ppb. The deviation from chemical equilibrium in the upper vortex is much greater than that in the lower vortex. Imperfect mixing (reflected in non-zero values for the PSS defect) results in negative apparent chemical ozone production, representing a systematic error if such an approach is applied to obtain ozone production rates within a poorly-mixed environment close to NO_x emissions sources. The substantial magnitude of the apparent ozone loss rate, relative to those encountered in the wider boundary layer / free troposphere, further suggests that even at some distance from fresh emissions, mixing-derived PSS defects may limit this approach in inferring chemical ozone production. This study demonstrates an approach to quantify parameters for a simplified two-box model, which could support traffic management and urban planning strategy or personal exposure assessment. A challenging research task for future study is to incorporate complex chemical mechanisms and consider various aspect ratios and wind speeds.

Acknowledgements

JZ thanks to the University of Birmingham for the award of a Li Siguang Scholarship, which is offered in partnership with the China Scholarship Council (CSC). The computations described herein were performed using the University of Birmingham's BlueBEAR HPC service (http://www.bear.bham.ac.uk), which was purchased through HEFCE SRIF-3 funds.

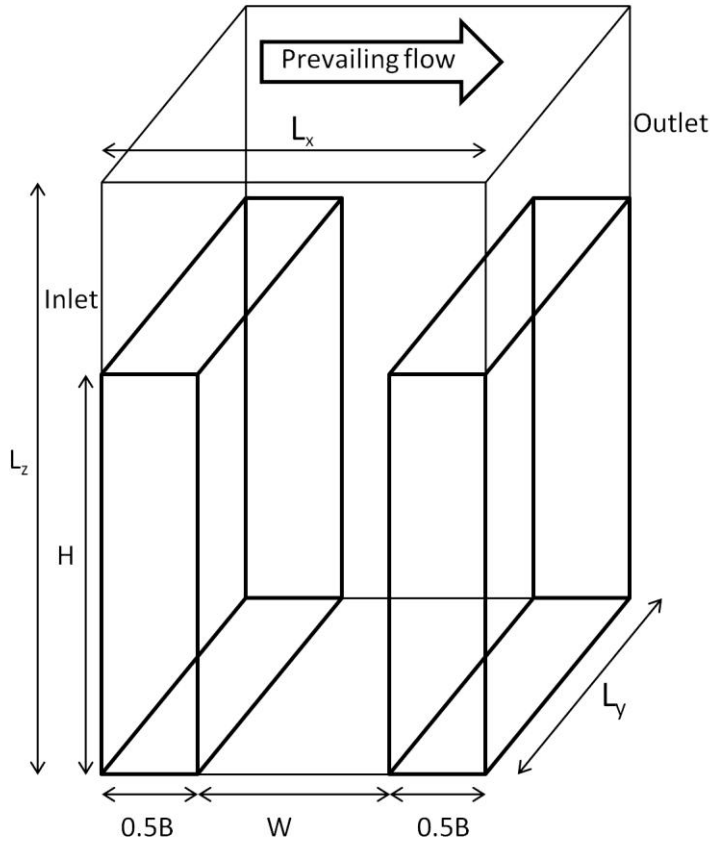

Fig. 1 Schematic diagram of the computational domain where L_x=36 m, L_y=40 m and L_z=112 m. H (=36 m) is the building height, W (=18 m) is the street width and B (=18 m) is the building width.

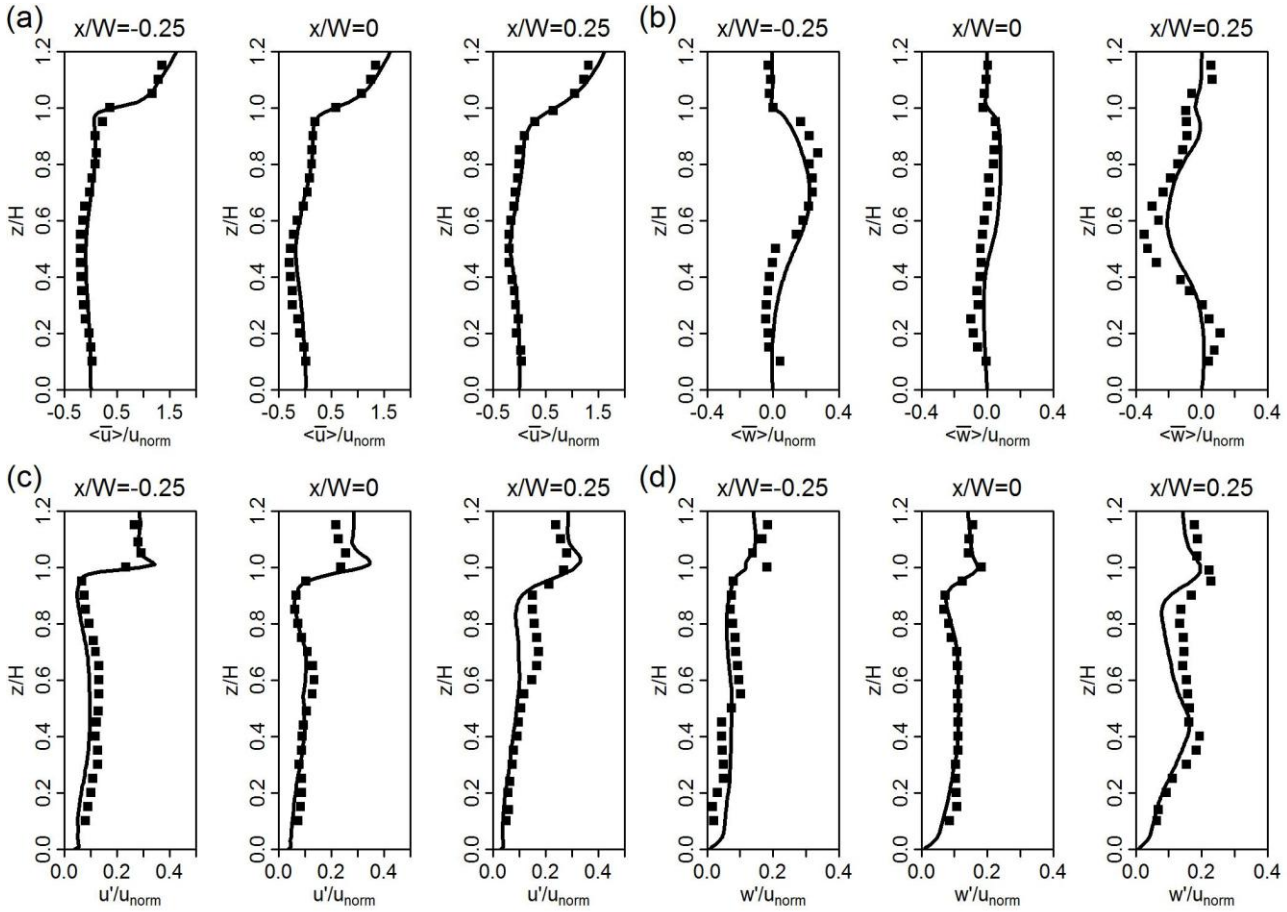

Fig 2. Comparison of the vertical profiles of the normalized averaged streamwise and vertical velocities and their fluctuations at the upstream (*x*/W=-0.25), centre (*x*/W=0) and downstream position (*x*/W=0.25) for the deep street canon with an aspect ratio of 2: (a) $\langle \overline{u} \rangle / u_{norm}$, (b) $\langle \overline{w} \rangle / u_{norm}$, (c) $u^{'} / u_{norm}$ and (d) $w^{'} / u_{norm}$. Solid lines represent the current LES simulation; Dark squares denote the water-channel experiment carried out by Li et al. (2008a).

430 (a) (b)

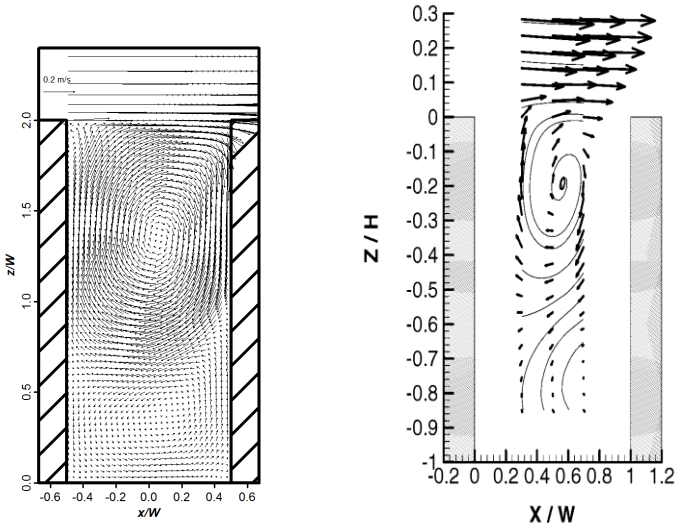

431

432 Fig 3. Vortex structure in the (a) current LES simulation (b) wind tunnel experiment carried out by (Kovar-Panskus et

433 al., 2002).

434

435

436

437

438

439

440

441

442

443

444

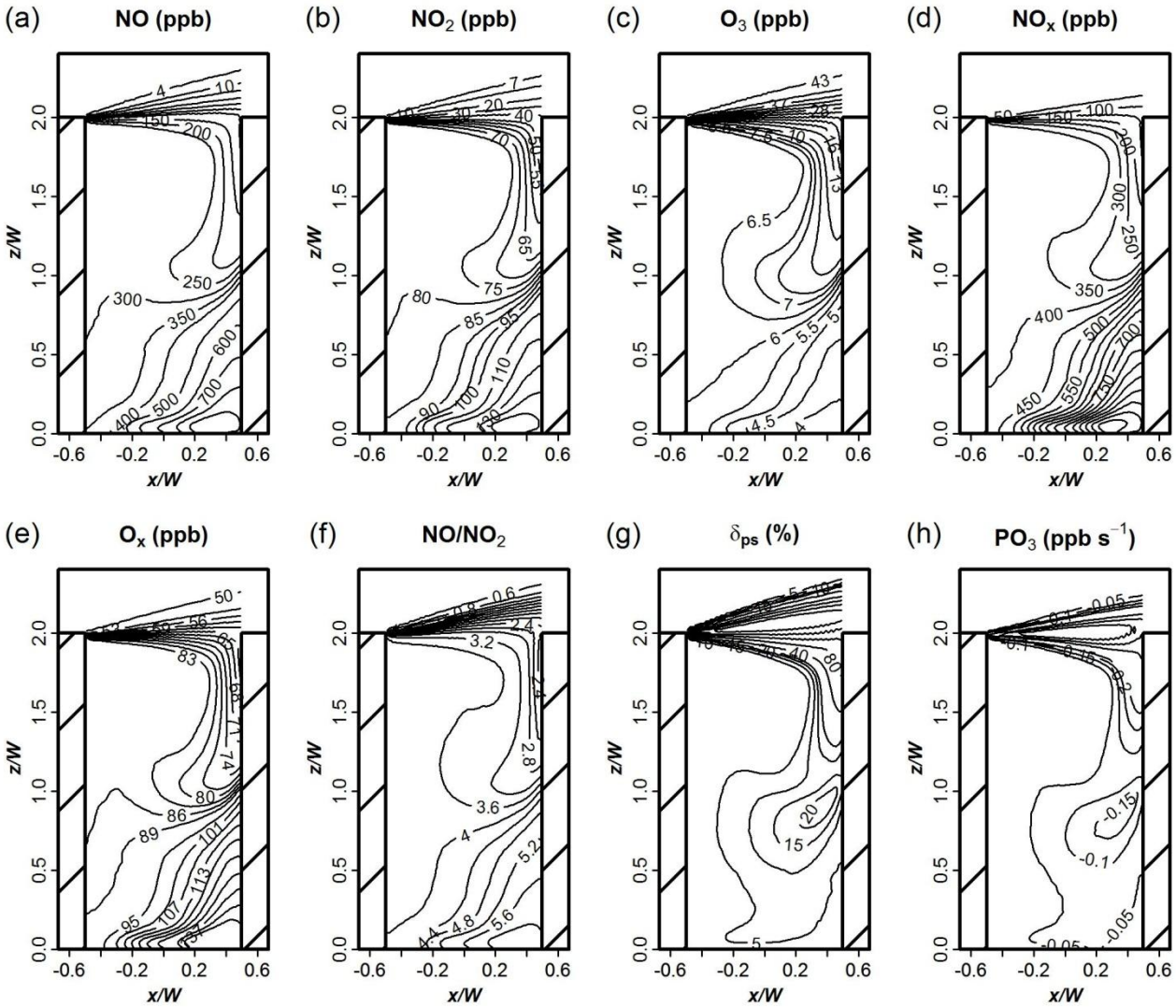

Fig. 4 Contour plots of the spatially and temporally averaged [see Equation (23)] (a) $\langle \overline{NO} \rangle$, (b) $\langle \overline{NO_2} \rangle$, (c) $\langle \overline{O_3} \rangle$, (d) $\langle \overline{NO_x} \rangle$, (e) $\langle \overline{O_x} \rangle$, (f) $\langle \overline{NO} \rangle / \langle \overline{NO_2} \rangle$, (g) d_{ps} and (h) PO_3.

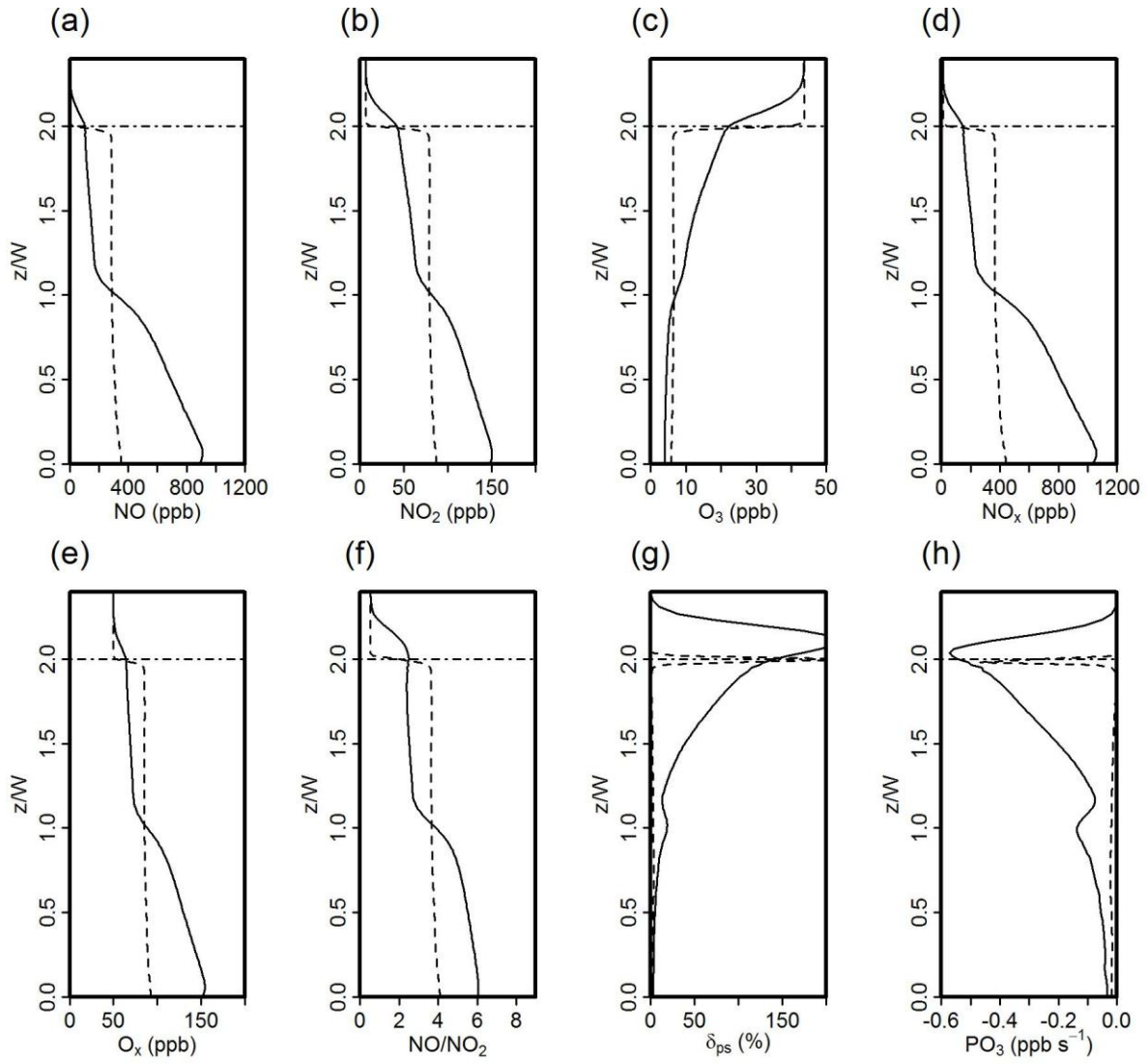

Fig. 5 Vertical profiles of the spatially and temporally averaged [see Equation (23)] (a) $\langle\overline{NO}\rangle$, (b) $\langle\overline{NO_2}\rangle$, (c) $\langle\overline{O_3}\rangle$, (d) $\langle\overline{NO_x}\rangle$, (e) $\langle\overline{O_x}\rangle$ and (f) $\langle\overline{NO}\rangle/\langle\overline{NO_2}\rangle$, (g) d_{ps} and (h) PO_3 along the leeward wall represented by the dash lines, and along the windward wall represented by the solid lines.

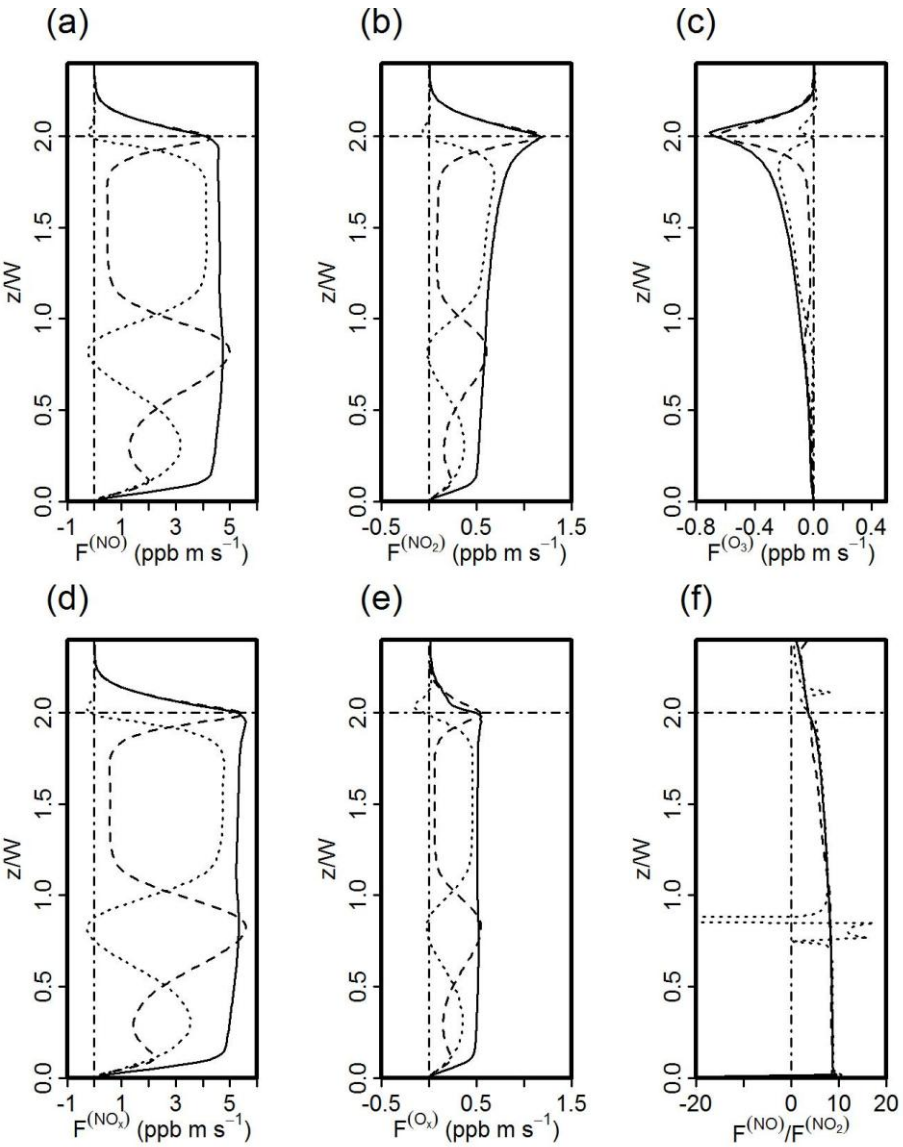

463

464 Fig. 6 Vertical profiles of the spatially and temporally averaged total, turbulent and advective fluxes for (a) NO, (b)

465 NO_2 , (c) O_3, (d) NO_x, (e) O_x and (f) NO/NO_2 averaged across the canyon. The total, turbulent and advective fluxes for

466 each quantity are represented by the solid, dash and dotted lines, respectively.

467

468

469

470

471

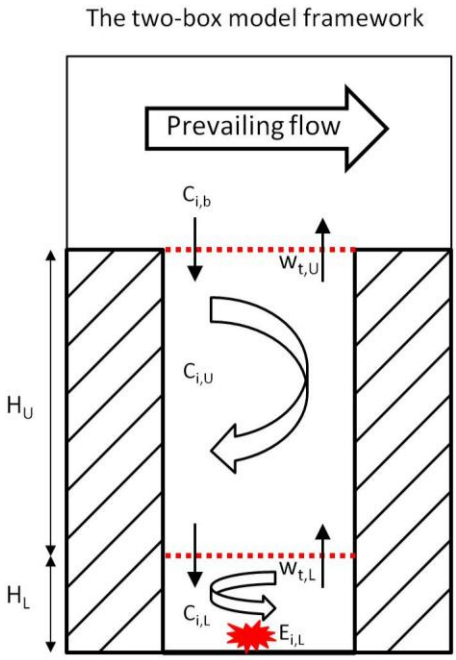

Fig. 7 Sketch of the two-box model framework. $c_{i,L}$ (ppb), $c_{i,U}$ (ppb) and $c_{i,b}$ (ppb) are the concentrations of ith species (i=NO, NO_2 and O_3) in the lower box, upper box, and overlying background atmosphere, respectively; H_L (m) and H_U (m) are the height of the lower and upper boxes, respectively; $w_{t,L}$ (m s^{-1}) is the exchange velocity between the lower and upper boxes, and $w_{t,U}$ (m s^{-1}) is the exchange velocity between the upper box and the overlying background atmosphere; and $E_{i,L}$ (ppb s^{-1}) is the emission rates of ith species.

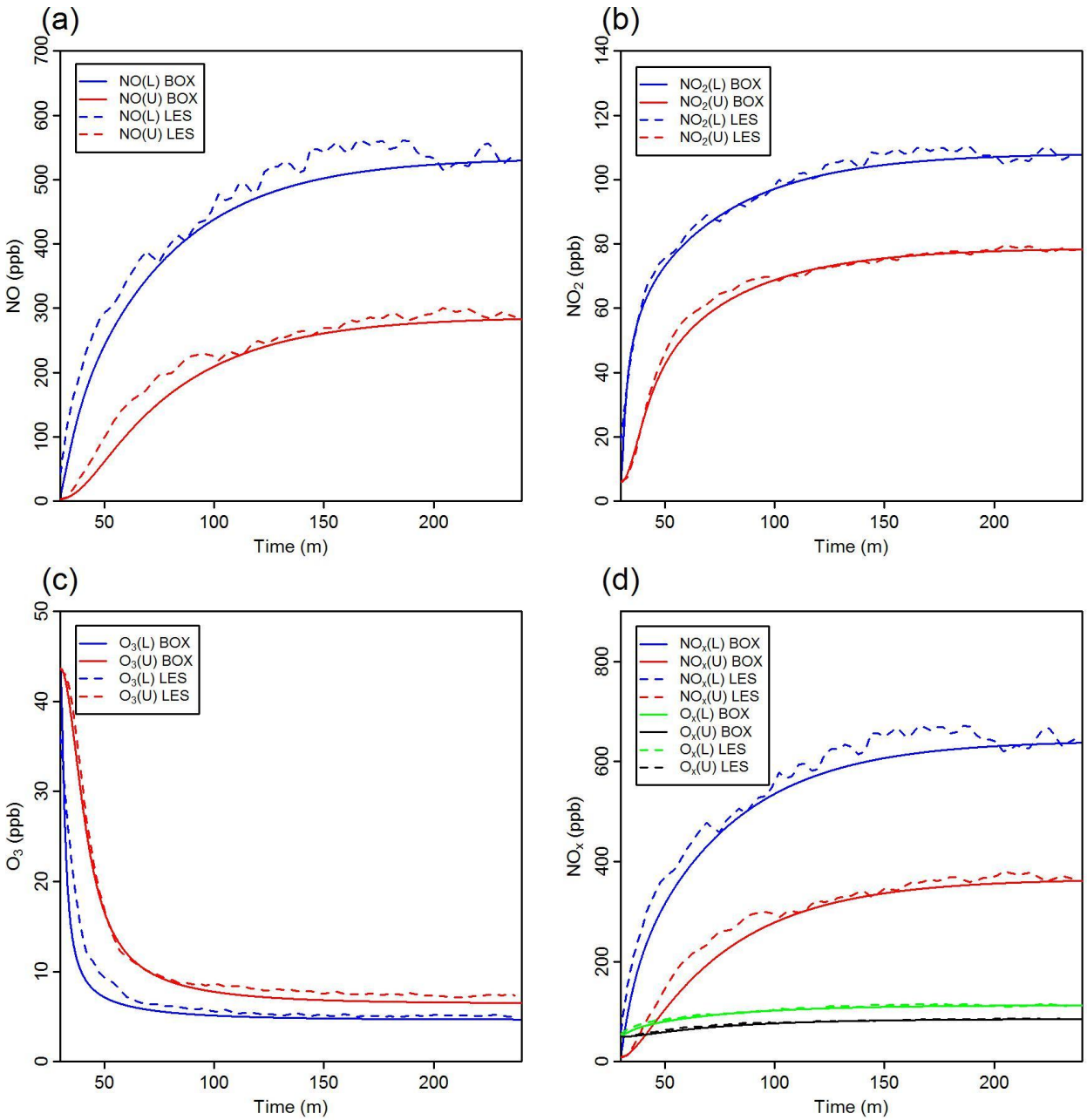

485

486 Fig. 8 Time evolution of the volume averaged mixing ratios of (a) NO, (b) NO_2, (c) O_3 and (d) NO_x and O_x calculated
487 using the LES simulation (LES) and the two-box model (BOX), respectively. 'L' represents the lower box while 'U'
488 represents the upper box.

489

490

491

492

References:

Baik, J.-J., Kang, Y.-S., Kim, J.-J., 2007. Modeling reactive pollutant dispersion in an urban street canyon. Atmospheric Environment 41, 934-949.

Baker, J., Walker, H.L., Cai, X.M., 2004. A study of the dispersion and transport of reactive pollutants in and above street canyons - a large eddy simulation. Atmospheric Environment 38, 6883-6892.

Boulter, P.G., Barlow, T.J., S., L., S., M.I., 2009b. Emission factors 2009: Report 1-a review of methods for determining hot exhaust emission factors for road vehicles. TRL:Wokingham,UK.

Bright, V.B., Bloss, W.J., Cai, X.M., 2013. Urban street canyons: Coupling dynamics, chemistry and within-canyon chemical processing of emissions. Atmospheric Environment 68, 127-142.

Cai, X.M., Barlow, J.F., Belcher, S.E., 2008. Dispersion and transfer of passive scalars in and above street canyons - Large-eddy simulations. Atmospheric Environment 42, 5885-5895.

Carpenter, L.J., Clemitshaw, K.C., Burgess, R.A., Penkett, S.A., Cape, J.N., McFadyen, G.C., 1998. Investigation and evaluation of the NO_x/O_3 photochemical steady state. Atmospheric Environment 32, 3353-3365.

Caton, F., Britter, R.E., Dalziel, S., 2003. Dispersion mechanisms in a street canyon. Atmospheric Environment 37, 693-702.

Chang, C.H., 2006. Computational fluid dynamics simulation of concentration distributions from a point source in the urban street canyons. J. Aerosp. Eng. 19, 80-86.

Garmory, A., Kim, I.S., Britter, R.E., Mastorakos, E., 2009. Simulations of the dispersion of reactive pollutants in a street canyon, considering different chemical mechanisms and micromixing. Atmospheric Environment 43, 4670-4680.

Jiang, Y., Liu, H., Sang, J., Zhang, B., 2007. Numerical and experimental studies on flow and pollutant dispersion in urban street canyons. Advances in Atmospheric Sciences 24, 111-125.

Kikumoto, H., Ooka, R., 2012. A numerical study of air pollutant dispersion with bimolecular chemical reactions in an urban street canyon using large-eddy simulation. Atmospheric Environment 54, 456-464.

Kovar-Panskus, A., Louka, P., Sini, J.F., Savory, E., Czech, M., Abdelqari, A., Mestayer, P.G., Toy, N., 2002. Influence of geometry on the mean flow within urban street canyons - A comparison of wind tunnel experiments and numerical simulations. Water, Air and Soil Pollution: Focus 2, 365-380.

Kumar, P., Fennell, P., Britter, R., 2008. Effect of wind direction and speed on the dispersion of nucleation and accumulation mode particles in an urban street canyon. Science of the Total Environment 402, 82-94.

Kwak, K.H., Baik, J.J., 2012. A CFD modeling study of the impacts of NOx and VOC emissions on reactive pollutant dispersion in and above a street canyon. Atmospheric Environment 46, 71-80.

Kwak, K.H., Baik, J.J., Lee, K.Y., 2013. Dispersion and photochemical evolution of reactive pollutants in street canyons. Atmospheric Environment 70, 98-107.

Li, X.-X., Leung, D.Y.C., Liu, C.-H., Lam, K.M., 2008a. Physical modeling of flow field inside urban street canyons. Journal of Applied Meteorology and Climatology 47, 2058-2067.

Li, X.-X., Liu, C.-H., Leung, D.Y.C., 2008b. Large-eddy simulation of flow and pollutant dispersion in high-aspect-ratio urban street canyons with wall model. Boundary-Layer Meteorology 129, 249-268.

Li, X.X., Liu, C.H., Leung, D.Y.C., 2009. Numerical investigation of pollutant transport characteristics inside deep urban street canyons. Atmospheric Environment 43, 2410-2418.

Liu, C.-H., Leung, D.Y.C., 2008. Numerical study on the ozone formation inside street canyons using a chemistry box model. Journal of Environmental Sciences-China 20, 832-837.

Liu, C.H., Leung, D.Y.C., Barth, M.C., 2005. On the prediction of air and pollutant exchange rates in street canyons of different aspect ratios using large-eddy simulation. Atmospheric Environment 39, 1567-1574.

Michioka, T., Sato, A., Takimoto, H., Kanda, M., 2011. Large-Eddy Simulation for the Mechanism of Pollutant Removal from a Two-Dimensional Street Canyon. Boundary-Layer Meteorology 138, 195-213.

Murena, F., Di Benedetto, A., D'Onofrio, M., Vitiello, G., 2011. Mass Transfer Velocity and Momentum Vertical Exchange in Simulated Deep Street Canyons. Boundary-Layer Meteorology 140, 125-142.

Murena, F., Favale, G., Vardoulakis, S., Solazzo, E., 2009. Modelling dispersion of traffic pollution in a deep street canyon: Application of CFD and operational models. Atmospheric Environment 43, 2303-2311.

Oke, T.R., 1987. Boundary Layer Climates. second ed Methuen, London.

OpenFOAM, 2012. http://www.openfoam.com/. Accessed May 2012.

Park, S.K., Kim, S.D., Lee, H., 2004. Dispersion characteristics of vehicle emission in an urban street canyon. Science of the Total Environment 323, 263-271.

Prajapati, S.K., Tripathi, B.D., Pathak, V., 2009. Distribution of vehicular pollutants in street canyons of Varanasi, India: a different case. Environmental Monitoring and Assessment 148, 167-172.

Sagrado, A.P.G., van Beeck, J., Rambaud, P., Olivari, D., 2002. Numerical and experimental modelling of pollutant dispersion in a street canyon. J. Wind Eng. Ind. Aerodyn. 90, 321-339.

Schlichting, H., Gersten, K., 2000. Boundary layer theory. Springer, Berlin.

Seinfeld, J.H., Pandis, S.N., 1998. Atmospheric chemistry and physics: from air pollution to climate change. Wiley, New York.

Solazzo, E., Vardoulakis, S., Cai, X., 2011. A novel methodology for interpreting air quality measurements from urban streets using CFD modelling. Atmospheric Environment 45, 5230-5239.

Tong, N.Y.O., Leung, D.Y.C., 2012. Effects of building aspect ratio, diurnal heating scenario, and wind speed on reactive pollutant dispersion in urban street canyons. Journal of Environmental Sciences-China 24, 2091-2103.

Volz-Thomas, A., Patz, H.W., Houben, N., Konrad, S., Mihelcic, D., Klupfel, T., Perner, D., 2003. Inorganic trace gases and peroxy radicals during BERLIOZ at Pabstthum: An investigation of the photostationary state of NO_x and O_3. Journal of Geophysical Research-Atmospheres 108.

Wood, E.C., Herndon, S.C., Onasch, T.B., Kroll, J.H., Canagaratna, M.R., Kolb, C.E., Worsnop, D.R., Neuman, J.A., Seila, R., Zavala, M., Knighton, W.B., 2009. A case study of ozone production, nitrogen oxides, and the radical budget in Mexico City. Atmospheric Chemistry and Physics 9, 2499-2516.

Xie, S.D., Zhang, Y.H., Li, Q., Tang, X.Y., 2003. Spatial distribution of traffic-related pollutant concentrations in street canyons. Atmospheric Environment 37, 3213-3224.

Zhong, J., Cai, X., Bloss, W.J., 2014. Modelling segregation effects of heterogeneous emissions on ozone levels in idealised urban street canyons: Using photochemical box models Environmental Pollution 188, 132-143.